[(L$_n$)Ru{η^3-(tpdt)}] Complexes as Dithiolate Donors to Group 10 Metal Centers: Synthetic, Single-Crystal X-ray Diffraction and Electrochemical Studies {L$_n$ = η^6-C$_6$Me$_6$ (HMB) and η^5-C$_5$Me$_5$ (Cp*); tpdt = S(CH$_2$CH$_2$S)$_2$}

Richard Y. C. Shin, Geok Kheng Tan, Lip Lin Koh, and Lai Yoong Goh*

Department of Chemistry, National University of Singapore, Kent Ridge, Singapore 119260

Richard D. Webster

Research School of Chemistry, Australian National University, Canberra, ACT 0200, Australia

Received August 1, 2004

Trinuclear mixed metal cationic complexes of Ru−Pd, [{(L$_n$)Ru(μ-η^2:η^3-tpdt)}$_2$Pd]$^{2+}$ (**4A**, L$_n$ = HMB; **8**, L$_n$ = Cp*), and of Ru−Pt, [{(L$_n$)Ru(μ-η^2:η^3-tpdt)}$_2$Pt]$^{2+}$ (**5B**, L$_n$ = HMB; **9**, L$_n$ = Cp*), containing bare bridging M(II) (M = Pd, Pt) centers, are formed from the reaction of [(HMB)Ru^{II}(η^3-tpdt)] (**1**) and [Cp*Ru^{III}(η^3-tpdt)] (**2**) (tpdt ≡ S(CH$_2$CH$_2$S)$_2$) with Pd(MeCN)$_2$Cl$_2$ (or PdCl$_2$) and PtCl$_2$, respectively. With Pt(PPh$_3$)$_2$Cl$_2$, both **1** and **2** displace the chloro ligands, thus forming dinuclear complexes [{(HMB)Ru(μ-η^2:η^3-tpdt)}{Pt(PPh$_3$)$_2$}]$^{2+}$ (**6**) and [{(Cp*)Ru(μ-η^2:η^3-tpdt)}{Pt(PPh$_3$)$_2$}]$^{2+}$ (**10**), in which Pt is coordinated to two thiolate atoms and two PPh$_3$ ligands in a four-coordinate planar geometrical environment. X-ray diffraction analyses show that the arene complexes **4A** and **5B** also possess four-coordinate planar geometry at the central metal atom. In the Cp* complexes, the central MS$_4$ moiety is tetrahedral for M = Pd, but planar for M = Pt, both metal centers being metal−metal bonded to the peripheral Ru atoms, presumably as dictated by the demands of the 18e rule. Electrochemical studies show that complexes **8** and **9** and the Ni analogues of **4A** and **8**, viz., **3** and **7**, respectively, can be reduced in two one-electron steps and oxidized by one electron. The one-electron reduced and oxidized species are paramagnetic, and EPR spectra were obtained of the species in frozen solutions. The electrochemical data indicate that the Pd- and Pt-containing compounds show intermediate electron delocalization between the two Ru atoms, indicative of a class II system, while the Ni-containing analogues show extensive electron delocalization between the Ru atoms, indicative of a class III system.

Introduction

Transition metal complexes containing sulfur donor ligands command a continuing interest on account of their relevance to biological and industrial processes.[1] In particular, hetero-bimetallic compounds are of special significance in applications as catalyst precursors in homogeneous catalysis or as models in heterogeneous catalysts.[2] The role of bridging monothiolates (RS$^-$) in these bi- or polynuclear compounds is prevalent;[3] however, the occurrence of bridging dithiolate ligands (−SRS−) is scarce,[4] and that of bridging dithiolate-thioether ligands such as 3-thiapentane-1,5-dithiolate, S(CH$_2$CH$_2$S$^-$)$_2$ (tpdt), is even rarer. There are a few di- and trinuclear homometallic coordination compounds reported to date with bonding modes a and b, shown in Chart 1.

Organometallic complexes containing bridging tpdt were virtually unknown until our recent reports of the role of complexes **1** and **2** as chelate metallodithiolate ligands in the formation of the dinuclear complexes **D**[8] of type "a" bonding, **E**−**G** of type "b" bonding, and the triruthenium complex **H** in which tpdt bridges in a new type c (μ_3-η^1: η^1: η^3-) bonding mode.[8−11] This paper describes the reactivity of **1** and **2** toward some group 10 metal systems, with emphasis on Pd and Pt.

* To whom correspondence should be addressed. E-mail: chmgohly@nus.edu.sg. Fax: (+65) 6779 1691.

(1) See, for instance, the following and the references therein: (a) *Transition Metal Sulfur Chemistry−Biological and Industrial Significance*; ACS Symposium Series 653, Stiefel, E. I., Matsumoto, K., Eds.; 1996. (b) Howard, J. B.; Rees, D. C. *Chem. Rev.* **1996**, *96*, 2965. (c) Sellman, D.; Sutter, J. *Acc. Chem. Res.* **1997**, *30*, 460. (d) Burgess, B. K.; Lowe, D. J. *Chem. Rev.* **1996**, *96*, 2983. (e) Dubois, M. R. *Chem. Rev.* **1989**, *89*, 1. (f) Curtis, M. D.; Druker, S. H. *J. Am. Chem. Soc.* **1997**, *119*, 1027. (g) Bianchini, C.; Meli, A. *Acc. Chem. Res.* **1998**, *31*, 109. (h) Sánchez-Delgado, R. A. *J. Mol. Catal.* **1994**, *86*, 287. (i) Holm, R. H.; Ciurli, S.; Weigel, J. A. *Prog. Inorg. Chem*. **1990**, *38*, 1. (j) Shibahara, T. *Coord. Chem. Rev*. **1993**, *123*, *73*. (k) Mathur, P. *Adv. Organomet. Chem.* **1997**, *41*, 243. (l) Ogino, H.; Inomata, S.; Tobita, H. *Chem. Rev*. **1998**, *98*, 2093.

(2) (a) Braunstein, P.; Rosé, J. In *Comprehensive Organometallic Chemistry II*; Wilkinson, G., Stone, F. G. A., Abel, E. W., Eds.; Pergamon: Oxford, 1995; Vol. 10, p 351. (b) Adams, R. D., Herrmann, W. A., Eds. The Chemistry of Heteronuclear Clusters and Multimetallic Catalysts. In *Polyhedron* **1988**, *7*, 2251. (c) Wheatley, N.; Kalck, P. *Chem. Rev.* **1999**, *99*, 3379. (d) Guczi, L. In *Metal Clusters in Catalysis*; Gates, B. C., Guczi, L., Knozinger, H., Eds.; Elsevier: New York, 1986. (e) Sinfelt, J. H. In *Bimetallic Catalysts: Discoveries, Concepts and Applications*; Wiley: New York, 1983. (f) Xiao, J.; Puddephat, R. J. *Coord. Chem. Rev.* **1995**, *143*, 457. (g) Holt, M. S.; Wilson, W. L.; Nelson, J. H. *Chem. Rev.* **1989**, *89*, 11.

10.1021/om049407t CCC: $27.50
Publication on Web 11/24/2004

Chart 1. Tpdt-Bridged Coordination Compounds

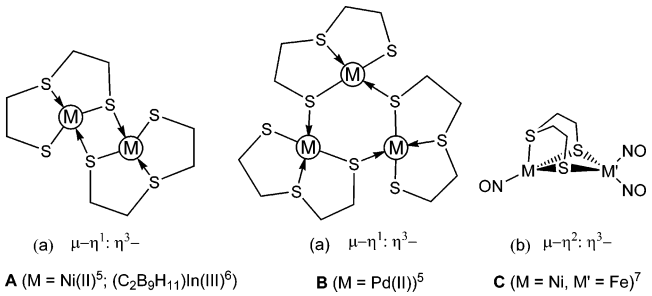

A (M = Ni(II)[5]; $(C_2B_9H_{11})$In(III)[6]) **B** (M = Pd(II))[5] **C** (M = Ni, M′ = Fe)[7]

Chart 2. Tpdt-Bridged Organoruthenium Complexes

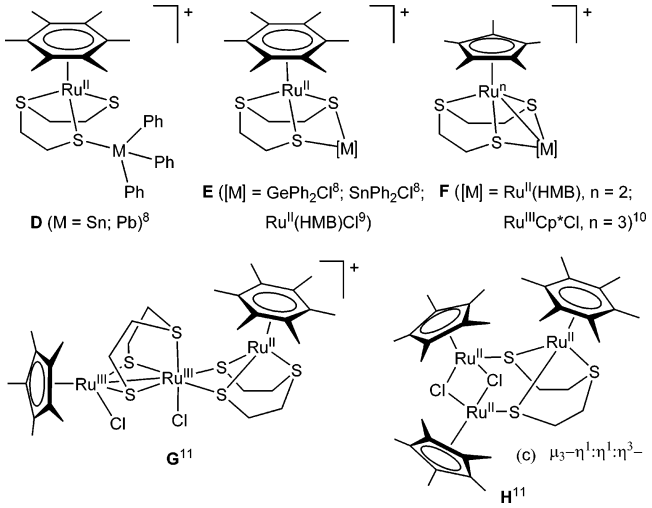

D (M = Sn; Pb)[8] **E** ([M] = $GePh_2Cl$[8]; $SnPh_2Cl$[8]; Ru^{II}(HMB)Cl[9]) **F** ([M] = Ru^{II}(HMB), n = 2; Ru^{III}Cp*Cl, n = 3)[10]

G[11] **H**[11]

Experimental Section

General Procedures. All reactions were carried out using conventional Schlenk techniques under an atmosphere of nitrogen or under argon in a M. Braun Labmaster 130 inert gas system. NMR spectra were measured on a Bruker 300 MHz FT NMR spectrometer (^{1}H at 300.14 MHz and ^{13}C at 75.43 MHz); ^{1}H and ^{13}C chemical shifts were referenced to residual solvent in the deutero-solvents CD_2Cl_2 and CD_3CN. Coupling constants (J) are in Hz. IR spectra were measured in KBr pellets in the range 4000−400 cm^{-1} on a BioRad FTS-165 FTIR instrument. FAB-mass spectra were obtained on a Finnigan Mat 95XL-T spectrometer. Voltammetric experiments were conducted with a computer-controlled Eco Chemie μAutolab III potentiostat. Solutions of electrogenerated compounds for the EPR experiments were prepared in a divided controlled potential electrolysis cell separated with a porosity no. 5 (1.0−1.7 μm) sintered glass frit. The working and auxiliary electrodes were identically sized Pt mesh plates symmetrically arranged with respect to each other with an Ag wire reference electrode (isolated by a salt bridge) positioned to within 2 mm of the surface of the working electrode. The electrolysis cell was jacketed in a glass sleeve and cooled to 233 K using a Lauda RL6 variable-temperature methanol-circulating bath. The volumes of both the working and auxiliary electrode compartments were approximately 20 mL each. The number of electrons transferred during the bulk oxidation process was calculated from

$$N = Q/nF \quad (1)$$

where N = no. of moles of starting compound, Q = charge (coulombs), n = no. of electrons, and F is the Faraday constant (96 485 C mol^{-1}). The electrolyzed solutions were transferred under vacuum into cylindrical 3 mm (id) EPR tubes that were immediately frozen in liquid N_2. EPR spectra were recorded on a Bruker ESP 300e spectrometer in a TE_{102} cavity at 10 K using liquid He cooling. Elemental analyses were performed by the microanalytical laboratory in-house. The compounds [(HMB)Ru(η^3-tpdt)] (**1**)[9] and [Cp*Ru(η^3-tpdt)] (**2**)[10] were prepared as described in our earlier reports. Other reagents were obtained from Aldrich and used as supplied. CH_3CN was distilled from calcium hydride and MeOH from freshly generated magnesium methoxide before use. All other solvents were distilled from sodium benzophenone ketyl.

(a) Reactions of 1. (i) With $PdCl_2$. To a stirred solution of **1** (30 mg, 0.07 mmol) in MeOH (10 mL) at room temperature was added solid $PdCl_2$ (9 mg, 0.05 mmol). An instantaneous color change from red to dark brown occurred. After 2 h the excess $PdCl_2$ was filtered, NH_4PF_6 (50 mg, 0.31 mmol) was added, and the mixture was stirred for 30 min, whereupon reddish brown solids of PF_6 salts and NH_4Cl precipitated out of solution. After filtration, the solids were extracted with CH_3CN (3 × 3 mL) and the extracts filtered through a disk of Celite (1.5 cm) to remove NH_4Cl and excess NH_4PF_6. The reddish brown filtrate was concentrated to ca. 5 mL and layered with ether; orange-red orthorhombic-shaped crystals (37 mg, 83.5% yield) of the PF_6 salt of [{(HMB)Ru(μ-η^2:η^3-tpdt)}$_2$Pd]$^{2+}$ (**4A/4B**) were obtained after 24 h at −30 °C. *For a 1:1 isomeric mixture:* ^{1}H NMR (δ, CD_3CN): SCH_2: 3.65−3.57 (7-line m, 2H), 3.43−3.30 (8-line m, 2H), 3.20−3.11 (5-line m, 2H), 2.90−2.81 (5-line m, 2H), 2.76−2.66 (8-line m, 2H), 2.50−2.40 (7-line m, 2H), 2.02−1.97 (5-line m, 2H), 1.83−1.74 (7-line m, 2H); C_6Me_6: 2.19, 2.09 (each s, 18H). ^{13}C NMR (δ, CD_3CN): C_6Me_6: 101.7, 101.6; SCH_2: 45.2, 44.3, 31.9, 31.0; C_6Me_6: 15.9, 15.5. FAB$^+$ MS: m/z 1083 [M − PF_6]$^+$, 939 [M − 2PF_6 + H]$^+$. FAB$^-$ MS: m/z 145 [PF_6]$^-$. Anal. Found: C, 31.9; H, 4.5; N, 0.3; S, 14.8. Calcd for $C_{32}H_{52}F_{12}P_2PdRu_2S_6$·0.5MeCN: C, 31.8; H, 4.3; N, 0.6; S, 15.4.

(3) See for instance the following and references therein: (a) Sappa, E.; Tiripicchio, A.; Braunstein, P. *Coord. Chem. Rev*. **1985**, *65*, 219. (b) Blower, P. J.; Dolworth, J. R. *Coord. Chem. Rev*. **1987**, *76*, 121. (c) Dance, I. G. *Polyhedron* **1986**, *5*, 1037. (d) Müller, A.; Diemann, E. In *Comprehensive Coordination Chemistry*; Wilkinson, G., Gillard, R. D., McCleverty, J. A., Eds.; Pergamon Press: Oxford, 1987; Vol. 2, Chapter 16.1, pp 526−531. (e) Stephan, D. W. *Coord. Chem. Rev*. **1989**, *95*, 41. (f) Janssen, M. D.; Grove, D. M.; Van Koten, G. *Prog. Inorg. Chem.* **1997**, *46*, 97. (g) Darensbourg, M. Y.; Pala, M.; Houliston, S. A.; Kidwell, K. P.; Spencer, D.; Chojnacki, S. S.; Reibenspies, J. H. *Inorg. Chem.* **1992**, *31*, 1487. (h) Yam, V. W.-W.; Wong, K. M.-C.; Cheung K.-K. *Organometallics* **1997**, *16*, 1729. (i) Delgado, E.; Garcíia, M. A.; Gutierrez-Puebla, E.; Hernández, E.; Mansilla, N.; Zamora, F. *Inorg. Chem.* **1998**, *37*, 6684. (j) Sánchez, G.; Ruiz, F.; Serrano, J. L.; Ramírez de Arellano, M. C.; López, G. *Eur. J. Inorg. Chem.* **2000**, *8*, 2185. (k) Nakahara, N.; Hirano, M.; Fukuoka, A.; Komiya, S. *J. Organomet. Chem.* **1999**, *572*, 81. (l) Capdevila, M.; Gonzalez-Duarte, P.; Foces-Foces, C.; Hernandez Cano, F.; Martinez-Ripoll, M. *J. Chem. Soc., Dalton Trans.* **1990**, 143. (m) Rousseau, R.; Stephan, D. W. *Organometallics* **1991**, *10*, 3399. (n) Amador, U.; Delgado, E.; Forniés-Cámer, J.; Hernandez, E.; Lalinde, E.; Moreno, M. T. *Inorg. Chem.* **1995**, *34*, 5279.

(4) (a) Aggarwal, R. C.; Mitra, R. *Ind. J. Chem.* **1994**, *A33*, 55. (b) Nadasdi, T. T.; Stephan, D. W. *Inorg. Chem*. **1994**, *33*, 1532. (c) Singh, N.; Prasad, L. B. *Ind. J. Chem.* **1998**, *A37*, 169. (d) Forniés-Cámer, J.; Masdeu-Bultó, A. M.; Claver, C.; Cardin, C. J. *Inorg. Chem.* **1998**, *37*, 2626. (e) Forniés-Cámer, J.; Masdeu-Bultó, A. M.; Claver, C.; Tejel, C.; Ciriano, M. A.; Cardin, C. J. *Organometallics* **2002**, *21*, 2609. (f) Forniés-Cámer, J.; Masdeu-Bultó, A. M.; Claver, C. *Inorg. Chem. Commun.* **2002**, *5*, 351. (g) Forniés-Cámer, J.; Claver, C.; Masdeu-Bultó, A. M.; Cardin, C. J. *J. Organomet. Chem.* **2002**, *662*, 188.

(5) (a) Harley-Mason, J. *J. Chem. Soc.* **1952**, 146. (b) Barclay, G. A.; McPartlin, E. M.; Stephenson, N. C. *Inorg. Nucl. Chem. Lett.* **1967**, *3*, 397. (c) Barclay, G. A.; McPartlin, E. M.; Stephenson, N. C. *Aust. J. Chem.* **1968**, *21*, 2669.

(6) Kim, J.-H.; Huang, J.-W.; Park, Y.-W.; Do, Y. *Inorg. Chem.* **1999**, *38*, 353.

(7) Liaw, W.-F.; Chiang, C.-Y.; Lee, G.-H.; Peng, S.-M.; Lai, C.-H.; Darensbourg, M. Y. *Inorg. Chem.* **2000**, *39*, 480.

(8) Shin, R. Y. C.; Vittal, J. J.; Zhou, Z.-Y.; Koh, L. L.; Goh, L. Y. *Inorg. Chim. Acta* **2003**, *352*, 220; **2004**, *357*, 635.

(9) Shin, R. Y. C.; Bennett, M. A.; Goh, L. Y.; Chen, W.; Hockless, D. C. R.; Leong, W. K.; Mashima, K.; Willis, A. C. *Inorg. Chem.* **2003**, *42*, 96.

(10) Goh, L. Y.; Teo, M. E.; Khoo, S. B.; Leong, W. K.; Vittal, J. J. *J. Organomet. Chem*. **2002**, *664*, 161.

(ii) With $PdCl_2(CH_3CN)_2$. A similar reaction of **1** (12 mg, 0.03 mmol) in MeOH (3 mL) with solid $PdCl_2(CH_3CN)_2$ (8 mg, 0.03 mmol) for 30 min, followed by metathesis with NH_4PF_6 (10 mg, 0.06 mmol) and a similar workup, gave reddish brown orthorhombic-shaped crystals (10 mg, 56.4% yield) of (**4A/4B**)$(PF_6)_2$ after 2 days at −30 °C.

(iii) With $PtCl_2$. To a stirred reddish orange solution of **1** (20 mg, 0.05 mmol) in MeOH (10 mL) was added solid $PtCl_2$ (7 mg, 0.03 mmol). The color changed gradually to yellow over 2 h at room temperature. Similar metathesis with NH_4PF_6 (40 mg, 0.24 mmol) with a similar subsequent workup gave yellow crystalline solids (22 mg, 69.4% yield) of the PF_6 salt of $[\{(HMB)Ru(\mu\text{-}\eta^2\text{:}\eta^3\text{-tpdt})\}_2Pt]^{2+}$ (**5A/5B**) after 2 days at −30 °C. *For a 1:1 isomeric mixture:* ^{1}H NMR (δ, CD_2Cl_2): SCH_2: 3.80−3.70 (8-line m, 2H), 3.52−3.44 (7-line m, 2H), 3.33−3.25 (7-line m, 2H), 3.13−3.05 (7-line m, 2H), 2.82−2.63 (11-line m, 4H), 1.95−1.87 (5-line m, 3H), 1.74−1.64 (8-line m, 1H); C_6Me_6: 2.17, 2.09 (each s, 18H). ^{13}C NMR (δ, CD_3CN): C_6-Me_6: 102.0, 101.9; SCH_2: 45.1, 43.8, 32.7, 31.2; C_6Me_6: 15.7, 15.4. FAB$^+$ MS: *m/z* 1171 $[M - PF_6]^+$, 1027 $[M - 2PF_6 + H]^+$, 999 $[M - 2PF_6 - 2CH_2 + H]^+$, 938 $[M - 2PF_6 - S(CH_2)_4]^+$. FAB$^-$ MS: *m/z* 145 $[PF_6]^-$. Anal. Found: C, 29.9; H, 4.5; N, 0.8; S, 14.3. Calcd for $C_{32}H_{52}F_{12}P_2PtRu_2S_6$·MeCN: C, 30.1; H, 4.1; N, 1.0; S, 14.2.

(iv) With $PtCl_2(PPh_3)_2$. Into a stirred solution of **1** (14 mg, 0.03 mmol) in MeOH (5 mL) was added $PtCl_2(PPh_3)_2$ (27 mg, 0.03 mmol). A color change from red to yellow occurred within 30 min at room temperature. Metathesis with NH_4PF_6 (20 mg, 0.12 mmol), followed by workup procedures as described above, gave yellow needle-shaped crystals (41 mg, 85.3% yield) of the PF_6 salt of $[\{(HMB)Ru(\mu\text{-}\eta^2\text{:}\eta^3\text{-tpdt})\}\{Pt(PPh_3)_2\}]^{2+}$ (**6**) after a day at −30 °C. ^{1}H NMR (δ, CD_3CN): C_6H_5: 7.56−7.51 (m, 5H), 7.46−7.35 (m, 25H); SCH_2: 3.06−2.97 (7-line m, 2H), 2.53−2.44 (6-line m, 2H), 1.86−1.75 (10-line m, 2H), 0.96−0.85 (6-line m, 2H); C_6Me_6: 2.09 (s, 18H). ^{13}C NMR (δ, CD_3CN): C_6H_5: 135.3 (t, *ortho*-, $^2J_{PC}$ = 4.4 Hz), 133.0 (s, *para*-), 129.8 (t, *meta*-, $^3J_{PC}$ = 5.5 Hz), 127.2 (d, *ipso*-, $^1J_{PC}$ = 61.0 Hz); C_6Me_6: 103.2; SCH_2: 39.9, 31.3; C_6Me_6: 15.8. ^{31}P NMR (δ, CD_3-CN): PPh_3: 18.4 (J_{P-Pt} 2857 Hz), PF_6: −142.9 (septet, J_{P-F} 706 Hz). FAB$^+$ MS: *m/z* 1280 $[M - PF_6]^+$, 1135 $[M - 2PF_6]^+$, 873 $[M - 2PF_6 - PPh_3]^+$, 844 $[M - 2PF_6 - PPh_3 - 2CH_2 + H]^+$, 815 $[M - 2PF_6 - PPh_3 - 4CH_2 + 2H]^+$. FAB$^-$ MS: *m/z* 145 $[PF_6]^-$. Anal. Found: C, 43.6; H, 4.0; S, 6.7. Calcd for $C_{52}H_{56}F_{12}P_4PtRuS_3$: C, 43.8; H, 4.0; S, 6.8.

Complex **3**, the Ni analogue of **4A**, was obtained from $NiCl_2(PPh_3)_2$.[12]

(b) Reactions of 2. (i) With $PdCl_2$. To a stirred solution of **2** (50 mg, 0.13 mmol) in MeOH (15 mL) at room temperature was added solid $PdCl_2$ (20 mg, 0.11 mmol). The mixture immediately changed from purple to dark brown. After 1 h, the excess $PdCl_2$ was filtered; the filtrate was stirred with NH_4PF_6 (100 mg, 0.61 mmol) for 30 min. As different from reactions of **1** described above, precipitation of product species was not observed; hence the mixture was evacuated to dryness and the residue extracted with CH_3CN (3 × 3 mL). The extracts were filtered to remove excess NH_4PF_6 and NH_4Cl. The reddish brown filtrate was concentrated to ca. 5 mL and layered with ether; reddish brown orthorhombic-shaped crystals (71 mg, 94.1% yield) of the PF_6 salt of $[\{Cp^*Ru(\mu\text{-}\eta^2\text{:}\eta^3\text{-tpdt})\}_2Pd]^{2+}$ (**8**) were obtained after 3 days at −30 °C. ^{1}H NMR (δ, CD_3CN): SCH_2: 3.03 (br s, 8H), 2.74−2.66 (6-line m, 8H); C_5Me_5: 1.77 (s, 30H). ^{13}C NMR (δ, CD_3CN): C_5Me_5: 105.2; SCH_2: 42.0, 39.0; C_5Me_5: 10.1. FAB$^+$ MS: *m/z* 1028 $[M - PF_6 + H]^+$, 883 $[M - 2PF_6 + H]^+$, 827 $[M - PF_6 - 4CH_2]^+$. FAB-MS: *m/z* 145 $[PF_6]^-$. Anal. Found: C, 29.3; H, 3.9; N, 1.2; P, 4.6; S, 15.9. Calcd for $C_{28}H_{46}F_{12}P_2PdRu_2S_6$·MeCN: C, 29.7; H, 4.1; N, 1.2; P, 5.1; S, 15.8.

(ii) With $PdCl_2(CH_3CN)_2$. A reaction of **2** (20 mg, 0.05 mmol) in MeOH (8 mL) with solid $PdCl_2(CH_3CN)_2$ (14 mg, 0.05 mmol) after a similar workup gave, after crystallization for 2 days at −30 °C, reddish brown orthorhombic-shaped crystals (18 mg, 59.7% yield) of **8**$(PF_6)_2$.

(iii) With $PtCl_2$. To a stirred solution of **2** (50 mg, 0.13 mmol) in MeOH (15 mL) at room temperature was added solid $PtCl_2$ (30 mg, 0.11 mmol). The color changed from purple to dark blue after 5 min. After 1 h, the excess $PtCl_2$ was filtered, and workup procedures similar to those described above gave blackish blue crystals (67 mg, 82.5% yield) of the PF_6 salt of $[\{Cp^*Ru(\mu\text{-}\eta^2\text{:}\eta^3\text{-tpdt})\}_2Pt]^{2+}$ (**9**). ^{1}H NMR (δ, CD_3CN): SCH_2: 3.89−3.82 (4-line m, 4H), 3.57−3.51 (4-line m, 4H), 2.52−2.40 (6-line m, 4H), 2.10−1.99 (7-line m, 4H); C_5Me_5: 1.89 (s, 30H). ^{13}C NMR (δ, CD_3CN): C_5Me_5: 104.6; SCH_2: 47.0, 37.4; C_5Me_5: 11.0. FAB$^+$ MS: *m/z* 1118 $[M - PF_6 - H]^+$, 973 $[M - 2PF_6 - H]^+$, 916 $[M - 2PF_6 - 4CH_2]^+$. FAB$^-$ MS: *m/z* 145 $[PF_6]^-$. Anal. Found: C, 26.6; H, 3.6; P, 4.5; S, 15.1. Calcd for $C_{28}H_{46}F_{12}P_2PtRu_2S_6$: C, 26.6; H, 3.7; P, 4.9; S, 15.2.

Complex **7**, the Ni analogue of **8**, was obtained from $NiCl_2(PPh_3)_2$.[12]

(iv) With $PtCl_2(PPh_3)_2$. A similar reaction of **2** (20 mg, 0.05 mmol) in MeOH (10 mL) with solid $PtCl_2(PPh_3)_2$ (42 mg, 0.05 mmol) for 12 h at room temperature, followed by workup procedures as described above, led to isolation of blackish brown needle-shaped crystals (24 mg, 33.4% yield) of the PF_6 salt of $[\{(Cp^*)Ru(\mu\text{-}\eta^2\text{:}\eta^3\text{-tpdt})\}\{Pt(PPh_3)_2\}]^{2+}$ (**10**). ^{1}H NMR (δ, CD_3CN): SCH_2 + PPh_3 + C_5Me_5: 8.18 (s, br, $\nu_{1/2}$ ca. 173 Hz), 7.68 (s, br, $\nu_{1/2}$ ca. 27 Hz). FAB$^+$ MS: *m/z* 1253 $[M - PF_6]^+$, 1108 $[M - 2PF_6]^+$, 846 $[M - 2PF_6 - PPh_3]^+$. FAB$^-$ MS: *m/z* 145 $[PF_6]^-$. Anal. Found: C, 42.8; H, 3.8; S, 6.6. Calcd for $C_{50}H_{53}F_{12}P_4PtRuS_3$: C, 43.0; H, 3.8; S, 6.9.

Crystal Structure Determinations. The crystals were mounted on glass fibers. X-ray data were collected on a Bruker AXS SMART APEX CCD diffractometer, using Mo Kα radiation (λ = 0.71073 Å) at 223 K. The program SMART[13] was used for collecting the intensity data, indexing, and determination of lattice parameters, SAINT[13] was used for integration of the intensity of reflections and scaling, SADABS[14] was used for absorption correction, and SHELXTL[15] was used for space group and structure determination and least-squares refinements against F^2. The structures were solved by direct methods to locate the heavy atoms, followed by difference maps for the light, non-hydrogen atoms. The hydrogens were placed in calculated positions. Fluorine atoms of the PF_6^- anions of **6**, **8**, and **10** were disordered. The asymmetric unit of the crystal of **8** contains two cations, one of which shows disorder in the methylene carbons of the tpdt ligands. Two of the ethylene chains are disordered in one of the methylene carbons with 50:50 occupancy ratio, while the other two chains show disorder of one of the methylene carbons with 65:35 occupancy ratio. The structural metric data for **8** are given for the nondisordered cation. There is one acetonitrile molecule present as space-filling solvent in complexes **8** and **4A** (disordered), fractional acetonitrile molecules in **5B** and **6**, and two acetonitrile molecules in **9** (one of which is disordered and shares the same site as a H_2O molecule). Crystal data and refinement parameters are given in Table S1 in the Supporting Information.

Results and Discussion

Syntheses and Reaction Pathways. The reaction of $[(HMB)Ru^{II}(\eta^3\text{-tpdt})]$ (**1**) with 0.5−1.0 molar equiv of

(11) Shin, R. Y. C.; Ng, S. Y.; Tan, G. K.; Koh, L. L.; Khoo, S. B.; Goh, L. Y.; Webster, R. D. *Organometallics* **2004**, *23*, 547, and references therein.

(12) Shin, R. Y. C.; Teo, M. E.; Goh, L. Y.; Murray, K. S.; et al. Manuscript in preparation.

(13) *SMART* & *SAINT* Software Reference Manuals, version 5.0; Bruker AXS Inc.: Madison, WI, 1998.

(14) Sheldrick, G. M. *SADABS* software for empirical absorption correction; University of Göttingen: Germany, 2000.

(15) *SHELXTL* Reference Manual, version 5.1; Bruker AXS Inc.: Madison, WI, 1998.

Scheme 1

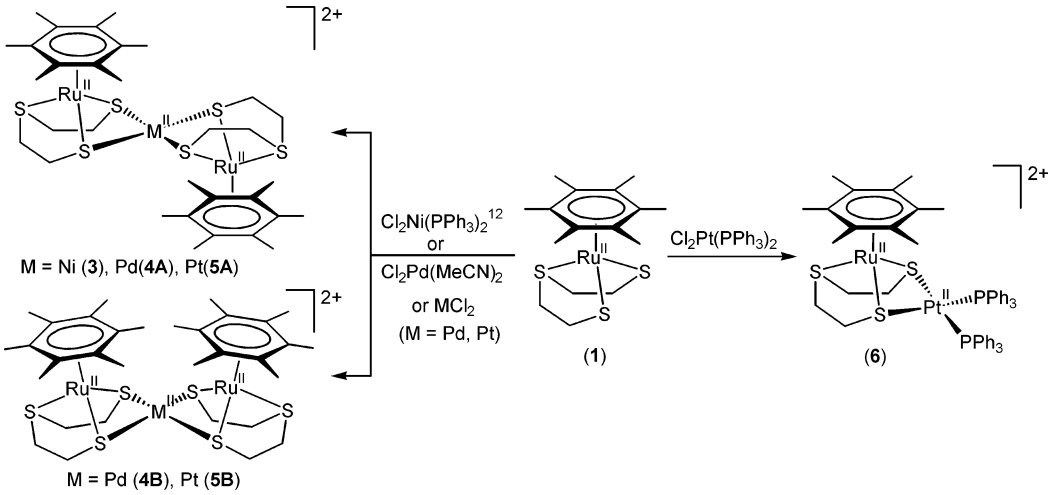

Scheme 2

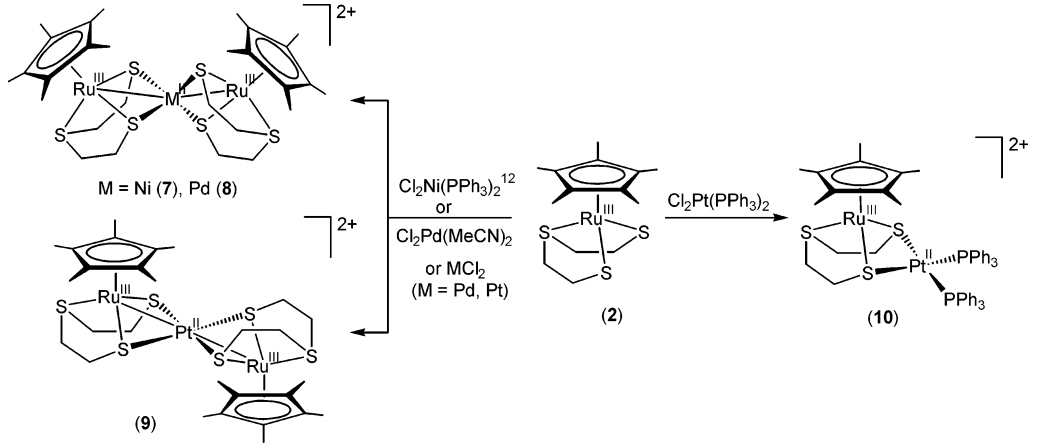

$(CH_3CN)_2PdCl_2$, $PdCl_2$, or $PtCl_2$ gives dicationic trinuclear complexes of formula $[\{(HMB)Ru(\mu\text{-}\eta^2\text{:}\eta^3\text{-tpdt})\}_2M]^{2+}$ (M = Pd (**4A/4B**), Pt (**5A/5B**)) in high yields. Thus the thiolate S atoms of **1** have acted as effective nucleophiles for the displacement of chloride or coordinated acetonitrile molecules at Pd or Pt. However, they are incapable of displacing PPh_3 from the coordination sphere of Pt, hence the formation of the dinuclear complex $[\{(HMB)Ru(\mu\text{-}\eta^2\text{:}\eta^3\text{-tpdt})\}\{Pt(PPh_3)_2\}]^{2+}$ (**6**) (Scheme 1).

Similarly, the thiolate S atoms of $[Cp^*Ru^{III}(\eta^3\text{-tpdt})]$ are capable of "stripping off" chloride and acetonitrile ligands but not PPh_3 from the coordination sphere of Pt, thus forming the dicationic dinuclear species **10** (Scheme 2).

Spectral and Structural Characterization. The molecular structures of **4A** and **5B** are illustrated in Figure 1, and selected bond parameters are given in Table 1. Both molecules possess a center of inversion at the central metal center, which is coordinated to four S donor atoms in planar configuration. The arene rings are oriented on opposite sides of the MS_4 plane in the Pd complex, but on the same side in the Pt complex (Scheme 1). Despite the slightly bigger size of Pt versus Pd (Δ = 0.02 Å), the Pd−S bond lengths (2.3407(8), 2.3310(9) Å) are longer than the Pt−S bond lengths

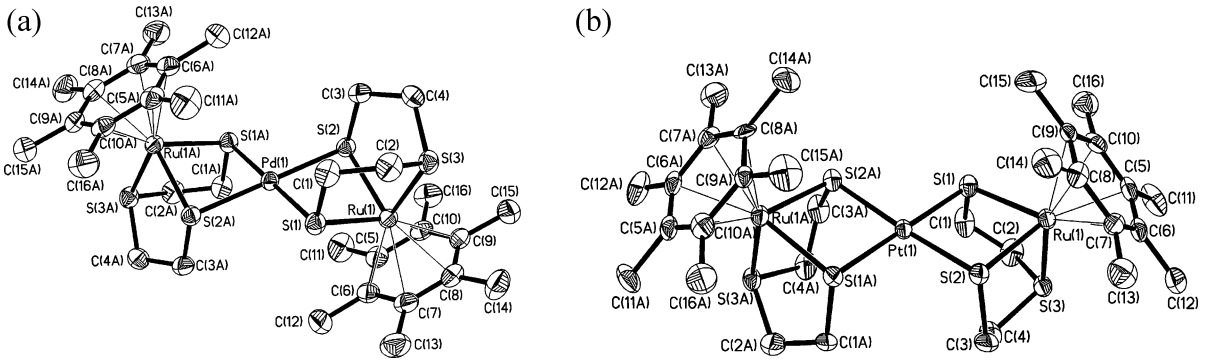

Figure 1. ORTEP plots for the molecular structures of the dications of (a) **4A** and (b) **5B**. Thermal ellipsoids are drawn at the 50% probability level. Hydrogen atoms are omitted for clarity.

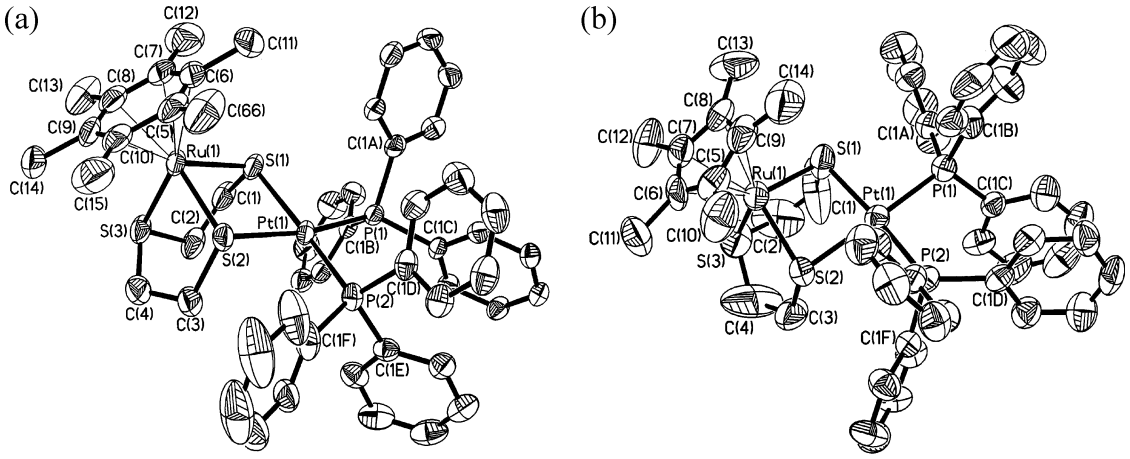

Figure 2. ORTEP plots for the molecular structures of the dications of (a) **6** and (b) **10**. Thermal ellipsoids are drawn at the 50% probability level. Hydrogen atoms are omitted for clarity.

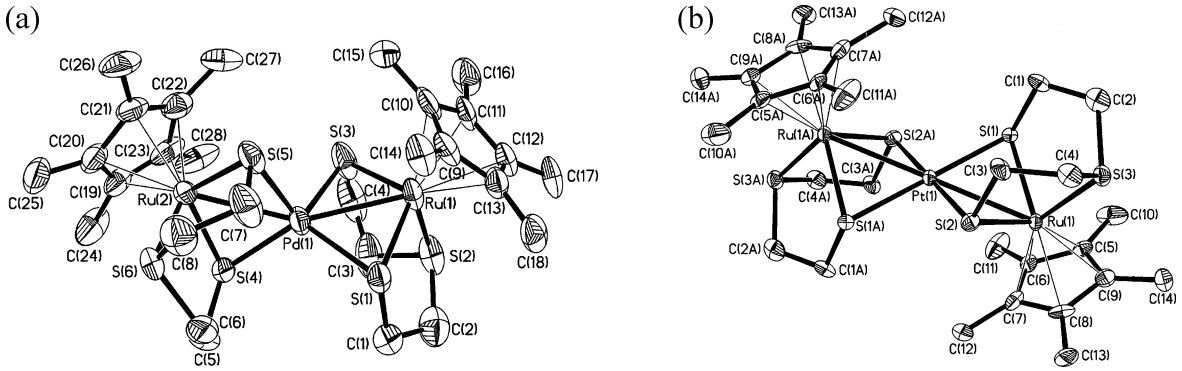

Figure 3. ORTEP plots for the molecular structures of the dications of (a) **8** and (b) **9**. Thermal ellipsoids are drawn at the 50% probability level. Hydrogen atoms are omitted for clarity.

Table 1. Selected Bond Lengths (Å) and Angles (deg) of HMB complexes

	4A[a]	**5B**[a]	**6**
Ru(1)−S(1)	2.3757(9)	2.363(3)	2.3647(19)
Ru(1)−S(2)	2.3685(9)	2.365(3)	2.362(2)
Ru(1)−S(3)	2.3255(9)	2.322(3)	2.320(2)
M(1)−S(1)	2.3407(8)	2.316(3)	2.4026(19)
M(1)−S(2)	2.3310(9)	2.314(3)	2.3620(18)
M(1)−P(1)			2.2951(18)
M(1)−P(2)			2.2970(19)
M(1)···Ru(1)	3.302	3.484	3.585
S(1)−Ru(1)−S(2)	83.60(3)	82.27(11)	81.94(7)
S(1)−Ru(1)−S(3)	86.58(3)	85.23(11)	86.90(7)
S(2)−Ru(1)−S(3)	86.78(3)	85.94(11)	85.36(8)
S(1)−M(1)−S(2)	85.20(3)	84.39(10)	81.14(7)
S(1)−M(1)−S(2A)	94.80(3)	95.64(11)	
Ru(1)−S(1)−M(1)	88.85(3)	96.25(11)	97.51(8)
Ru(1)−S(2)−M(1)	89.26(3)	96.24(11)	98.73(8)
S(1)−Pt(1)−P(1)			88.95(6)
S(2)−Pt(1)−P(2)			92.53(7)
P(1)−Pt(1)−P(2)			97.19(6)

[a] Molecule possesses center of inversion at M (Pd or Pt).

(2.316(3), 2.314(3) Å), consistent with an expected stronger bond with the larger atom. The Ru−S(thiolate) bond lengths in **4A** and **5B** average 2.3721(9) and 2.364(3) Å, respectively, while the Ru−S (thioether) distances are 2.3255(9) and 2.322(3) Å for the two analogues. In the dinuclear complex **6** (Figure 2a), donor groups at Pt are also arranged in planar configuration, with Pt−S bond lengths substantially longer ($\Delta = 0.087$, 0.048 Å) than equivalent bonds in **5B**; the Ru−S bond distances are very close to those in **5B**.

The ORTEP diagrams for the structures of **8** and **9** are shown in Figure 3, and their selected bond parameters given in Table 2. In the molecule of **8**, the Pd center is coordinated to four S donor atoms in a distorted tetrahedral geometry (Pd−S bonds of lengths 2.321(3)−2.460(3) Å and S−Pd−S angles of 103.56(9)−117.80(10)°) and is bonded to the Ru peripheral atoms (bond lengths 2.6758(10), 2.6833(11) Å), with Ru(1)−Pd(1)−Ru(2) equal to 152.94(4)°. The Ru−S distances are substantially shorter ($\Delta = 0.0495-0.0747$ Å) than their equivalents in the HMB analogue **4A**. The molecular structure of **9** differs markedly from that of **8**. A center of inversion exists at Pt, which is planar with respect to the four S donors and is only weakly bonded to the peripheral Ru atoms (Ru−Pt = 2.7818(12) Å, exceeds the sum of their covalent radii (2.55 Å) or atomic radii (2.73 Å)), with the three metal centers in linear alignment. The molecular structure of **10** (Figure 2b) resembles closely that of **6**, with differences in Ru−S(thiolate) and Pt−S bonds, which are shorter in **10**, resulting in a shorter Ru···Pt nonbonding distance ($\Delta = 0.424$ Å). Pt−P distances are slightly longer in **10**.

The presence of inversion centers at M in the molecular structures of the trinuclear Ru_2M complexes (M = Pd (**4**) and M = Pt (**5**)) is expected to result in equivalent arene rings. However, the proton and ^{13}C NMR spectra of both complexes are consistent with the presence of nonequivalent rings. We attribute this to the existence of both "trans" and "cis" isomers in **4** and **5**, though only "trans"-**4A** and "cis"-**5B** were structurally characterized

Table 2. Selected Bond Lengths (Å) and Angles (deg) of Cp* Complexes

8		9[a]		10	
Ru(1)−S(1)	2.301(3)	Ru(1)−S(1)	2.342(4)	Ru(1)−S(1)	2.308(4)
Ru(1)−S(2)	2.319(3)	Ru(1)−S(2)	2.337(4)	Ru(1)−S(2)	2.329(3)
Ru(1)−S(3)	2.273(3)	Ru(1)−S(3)	2.339(4)	Ru(1)−S(3)	2.326(4)
Pd(1)−S(1)	2.342(3)	Ru(1)−Pt(1)	2.7818(12)	Pt(1)−S(1)	2.374(3)
Pd(1)−S(3)	2.420(3)	Pt(1)−S(1)	2.327(4)	Pt(1)−S(2)	2.437(3)
Pd(1)−S(4)	2.321(3)	Pt(1)−S(2)	2.330(4)	Pt(1)−P(1)	2.301(3)
Pd(1)−S(5)	2.460(3)			Pt(1)−P(2)	2.313(3)
Pd(1)−Ru(1)	2.6758(10)			Pt(1)···Ru(1)	3.161
Pd(1)−Ru(2)	2.6833(11)				
Ru(2)−S(4)	2.294(3)				
Ru(2)−S(5)	2.272(3)				
Ru(2)−S(6)	2.316(3)				
S(1)−Ru(1)−S(2)	85.82(11)	S(1)−Ru(1)−S(2)	93.01(13)	S(1)−Ru(1)−S(2)	95.16(13)
S(1)−Ru(1)−S(3)	110.29(10)	S(1)−Ru(1)−S(3)	86.15(14)	S(1)−Ru(1)−S(3)	85.93(16)
S(2)−Ru(1)−S(3)	85.50(13)	S(2)−Ru(1)−S(3)	86.19(14)	S(2)−Ru(1)−S(3)	86.67(14)
S(1)−Pd(1)−S(3)	104.02(10)	S(1)−Pt(1)−S(2)	93.56(13)	S(1)−Pt(1)−S(2)	90.71(12)
S(1)−Pd(1)−S(4)	117.80(10)	S(1)−Pt(1)−S(2A)	86.44(13)	S(1)−Pt(1)−P(1)	87.56(12)
S(1)−Pd(1)−S(5)	110.34(10)	Ru(1)−S(1)−Pt(1)	73.14(11)	S(2)−Pt(1)−P(2)	84.20(11)
S(3)−Pd(1)−S(4)	111.83(11)	Ru(1)−S(2)−Pt(1)	73.16(11)	P(1)−Pt(1)−P(2)	97.53(11)
S(3)−Pd(1)−S(5)	109.22(12)	Ru(1)−Pt(1)−Ru(1A)	180.00(5)	Ru(1)−S(1)−Pt(1)	84.93(12)
S(4)−Pd(1)−S(5)	103.56(9)			Ru(1)−S(2)−Pt(1)	83.06(11)
S(4)−Ru(2)−S(5)	110.78(11)				
S(4)−Ru(2)−S(6)	85.52(11)				
S(5)−Ru(2)−S(6)	86.32(11)				
Ru(1)−Pd(1)−Ru(2)	152.94(4)				

[a] Molecule possesses center of inversion at M.

by single-crystal X-ray analysis. [In comparison, the Ni complex **3** exists as one isomer in both solution and solid states.[12]] The SCH_2 groups are seen as eight- and seven-line multiplets in the proton NMR spectra and as four signals in the range δ 31.0−45.2 in the ^{13}C NMR spectra. Unlike **4**, the (Cp*)Ru(III) analogue **8** exhibits resonances indicative of two equivalent Cp* rings as expected; likewise for **9**. The hindrance to the formation of two "geometrical" isomers in this case is not obvious. The proton NMR spectra show two multiple-line "clusters" for the SCH_2 groups of **8** but four such "clusters" for **9**. The well-resolved fine structure seen in the NMR spectra of these complexes is in agreement with 18-electron configurations at all three metal centers, by virtue of metal−metal bonds between the peripheral Ru atoms and the central Pd/Pt atom. In contrast paramagnetism arising from a 17-electron environment at Ru in the non metal−metal bonded complex **10** is manifested in broad featureless signals in the proton NMR spectrum and the absence of observable signals in the ^{13}C spectrum in the normal range. In comparison, it was observed that the dinuclear complex **6**, analogue of **10**, is diamagnetic (18e at Ru and 16e at Pt(II)), possessing well-defined proton and carbon resonances in the NMR spectra for the arene ring and thiolate ligand in the same range found for **5A/5B**.

Electrochemistry and EPR Spectroscopy. Cyclic voltammograms (CV) obtained at a GC electrode in 0.5 mM solutions of the PF_6 salts of **7**, **8**, and **9** in CH_2Cl_2 at 233 K are shown in Figure 4. All of the compounds displayed two well-defined chemically reversible reduction processes and one chemically reversible oxidation process. **8** displayed a third reduction process with greater current magnitude than either of the first two reduction processes (indicating that a higher number of electrons were transferred) at very negative potentials (~ -2.6 V vs Fc/Fc^+) that showed no reverse peak when the scan direction was reversed, suggesting chemical instability of the triply reduced species. **8** and **9** showed

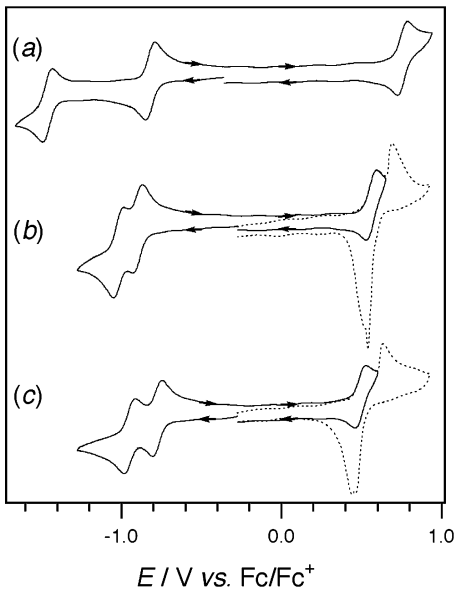

Figure 4. Cyclic voltammograms performed at a 1 mm diameter planar GC electrode in CH_2Cl_2 (0.25 M Bu_4NPF_6) at 233 K at a scan rate of 100 mV s^{-1} for 0.5 mM (a) **7**, (b) **8**, and (c) **9**.

an additional oxidation process at potentials immediately after the first oxidation process [Figure 4 (dashed lines)] that was indicative of an adsorption/stripping mechanism, presumably due to low solubility of the oxidized compounds.

8 and **9** displayed an interesting electrochemical response on Pt electrodes. The first (less negative) reduction process was identical on Pt and GC electrodes, while the second more negative process could barely be detected on Pt, with only a small drawn out wave being observed. An adsorption mechanism specific to Pt is not likely in this case because the first reductive electron transfer process was not affected by repetitive cycling even when the potential was extended past the second process. Instead the diminished current seen for the

Table 3. Cyclic Voltammetric Data Obtained at a Scan Rate of 100 mV s^{-1} at a 1 mm Diameter Glassy Carbon Electrode at 233 K in CH_2Cl_2 with 0.25 M Bu_4NPF_6 as the Supporting Electrolyte

	reduction processes[a]				oxidation processes[a]			
compound	E_p^{red}/V[b]	E_p^{ox}/V[c]	$E^r_{1/2}$/V[d]	ΔE/mV[e]	E_p^{ox}/V[c]	E_p^{red}/V[b]	$E^r_{1/2}$/V[d]	ΔE/mV[e]
7	−0.845	−0.787	−0.82	58				
	−1.491	−1.429	−1.46	62				
					+0.790	+0.725	+0.76	65
8	−0.928	−0.867	−0.90	61				
	−1.046	−0.983	−1.01	63				
					+0.597	+0.528	+0.56	69
9	−0.804	−0.745	−0.77	59				
	−0.982	−0.912	−0.95	70				
					+0.527	+0.459	+0.49	68
3	−1.360	−1.287	−1.32	73				
	−1.995	−1.895	−1.95	100				
					+0.498	+0.375	+0.44	123
4A/4B	−1.76							
					+0.624	+0.528	+0.58	96
5A/5B	−2.12							
					+0.59	+0.52	+0.56	70

[a] All potentials are relative to the ferrocene/ferrocenium redox couple. [b] E_p^{red} = reductive peak potential. [c] E_p^{ox}= oxidative peak potential. [d] $E^r_{1/2} = (E_p^{red} + E_p^{ox})/2$. [e] $\Delta E = |E_p^{ox} - E_p^{red}|$.

second reduction process was likely to be caused by an exceedingly slow rate of heterogeneous charge transfer on Pt. In contrast to **8** and **9**, the reduction processes of **7** appeared identical on Pt and GC electrodes.

Table 3 lists the reversible reduction potentials ($E^r_{1/2}$) that were calculated from CV data under conditions where the ratio of the oxidative (i_p^{ox}) to reductive (i_p^{red}) peak currents were equal to unity and using the relationship

$$E^r_{1/2} = (E_p^{ox} + E_p^{red})/2 \quad (2)$$

where E_p^{ox} and E_p^{red} are the anodic and cathodic peak potentials, respectively. In situations where no reverse peak was observed, only the peak potential is given. In most instances where the E_p^{ox} and E_p^{red} peak separation (ΔE) could be measured, the values obtained were close to that expected for a one-electron transfer (Table 3). By assuming that the diffusion coefficients for **7**−**9** are very similar, and by comparing the anodic and cathodic peak currents shown in Figure 4, it is reasonable to expect that the first two reduction processes and first oxidation process all occur by the same number of electrons (i.e., $n = 1$). Coulometry measurements (eq 1) made during exhaustive controlled potential electrolysis (CPE) experiments at 233 K for the first reduction and oxidation processes confirmed the transfer of one-electron per molecule. Most of the one-electron reduced and oxidized species were stable for at least 2−3 h at low temperatures (233 K) in CH_2Cl_2 and could be reversibly oxidized/reduced back to their starting materials.The CV responses obtained for solutions of the PF_6 salts of **3**, **4A/4B**, and **5A/5B** (Figure 5) were similar to those obtained for **7**−**9**. The Ni-containing compound **3** showed two reduction processes separated by several hundred mV (Figure 5a), similar to those observed for **7** (Figure 4a). **4A/4B** and **5A/5B** displayed one chemically irreversible reduction process, indicating that the reduced forms of those compounds were chemically unstable, which prevented the detection of the second reduction process (should it occur). **3**, **4A/4B**, and **5A/5B** all showed an oxidation process at positive potentials, although for **3** and **5A/5B** the peak shapes were complicated, suggesting steps in addition to simple electron transfer.

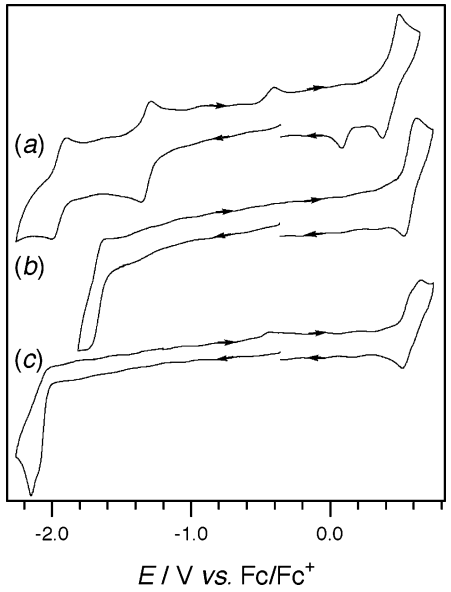

Figure 5. Cyclic voltammograms performed at a 1 mm diameter planar GC electrode in CH_2Cl_2 (0.25 M Bu_4NPF_6) at 233 K at a scan rate of 100 mV s^{-1} for 0.5 mM (a) **3**, (b) **4A/4B**, and (c) **5A/5B**.

For symmetrical compounds with more than one possible redox center, similar to Creutz-Taube type ions,[16] the separation in the electron transfer steps can be used to determine the comproportionation constant (K_c) that is a measure of the degree of interaction between the metal centers.

$$K_c = \exp[(E_1^\circ - E_2^\circ)F/RT] \quad (3)$$

For **3** and **7**, the difference in potential between the first and second reduction processes ($E_1^\circ - E_2^\circ$) is 0.63 and 0.64 V, respectively, which leads to a very high value of K_c of 10^{14} for the equilibrium

$$[\text{Ru-Ni-Ru}]^{2+} + [\text{Ru-Ni-Ru}]^0 \leftrightarrow 2[\text{Ru-Ni-Ru}]^+ \quad (4)$$

Values of $K_c > 10^6$ are considered to be indicative of a

(16) (a) Creutz, C.; Taube, H. *J. Am. Chem. Soc.* **1969**, *91*, 3988. (b) Creutz, C.; Taube, H. *J. Am. Chem. Soc.* **1973**, *95*, 1086.

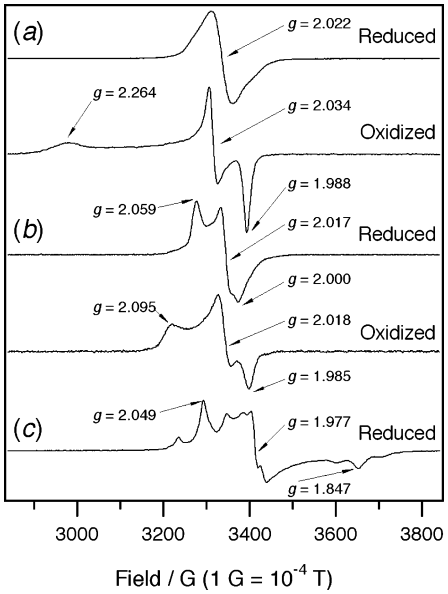

Figure 6. Continuous wave X-band EPR spectra obtained at 10 K with microwave frequency = 9.443 GHz and microwave power = 0.2 mW. The paramagnetic samples were prepared by one-electron controlled potential electrochemical reduction or oxidation of the starting materials in CH_2Cl_2 containing 0.5 M Bu_4NPF_6 at 233 K: (a) **7**, (b) **8**, and (c) **9**.

class III system (extensive delocalization) according to the Robin−Day scheme;[17] hence the redox properties must be considered in terms of a shared molecular orbital. However, for **8** and **9**, K_c values for the analogous equilibrium to reaction 4 can be calculated to be 10^2 and 10^4, respectively. Values $< 10^2$ are thought to be characteristic of class I systems where the unpaired electrons are essentially localized, while class II systems occur where $10^2 < K_c < 10^6$ and represent situations where there is intermediate delocalization.[17]

The well-defined cyclic voltammograms obtained for **7**−**9**, combined with the $n = 1$ values calculated during CPE experiments, indicated that those compounds were promising candidates for electrochemical-EPR spectroscopy. Since the starting materials were all nonparamagnetic but contained two formally Ru(III) ions, the diamagnetic ground states could be accounted for by pairing of one of the d^5 electrons from each Ru in a shared molecular orbital. Therefore, it was expected that the one-electron oxidation or reduction would remove the diamagnetism and produce a paramagnetic species. This was confirmed by EPR experiments performed on bulk electrolyzed solutions (see Experimental Section) where EPR spectra were obtained for most of the one-electron reduced and one-electron oxidized states (Figure 6). (The one-electron oxidized form of **9** did not yield an EPR spectrum, either because the compound adsorbed too strongly on the electrode surface or because it decomposed during the electrolysis.)

(17) Robin, M. B.; Day, P. *Adv. Inorg. Chem. Radiochem.* **1967**, *10*, 247.

Most of the EPR spectra showed features typical of compounds with rhombic (low symmetry) structure and displayed three *g*-values. If it is assumed that the unpaired electrons are delocalized (which is suggested by the diamagnetic state of the starting materials), the rhombic symmetry evident in the EPR spectra can be explained by the compounds existing in a distorted state in frozen solution at low temperatures or by the unpaired electron interacting extensively with the ruthenium atoms in a low-symmetry environment. The exception to this is the reduced form of the Ni compound that showed an isotropic shaped EPR spectrum (Figure 6a), suggesting a high degree of symmetry. The EPR spectra of frozen solutions of other paramagnetic heterobimetallic species often show broad lines with axial symmetry indicating the unpaired electron resides predominantly on the metal ions, rather than being ligand centered.[18]

Conclusion

The dithiolato donor atoms of η^3-tdpt in complexes of (HMB)Ru(II) (**1**) and Cp*Ru(III) (**2**) behave as effective metallo-chelates to bare Pd(II) and Pt(II) centers, giving rise to trinuclear mixed metal Ru_2Pd and Ru_2Pt complexes, respectively. X-ray diffraction analyses show that the trinuclear arene complexes possess four-coordinate square-planar geometry at the central metal atom. In comparison the central MS_4 moiety in the Cp* analogues is tetrahedral for M = Pd, but planar for M = Pt; in both these complexes there exist M−M bonds to the peripheral Ru centers, in accordance with the demands of the 18e rule. With $Pt(PPh_3)_2Cl_2$, **1** and **2** can only displace the chloro ligands, forming bis-(dithiolate)-bridged dinuclear complexes, in which Pt retains the two phosphine ligands, as well as its square-planar configuration. Electrochemical measurements show that the reduced forms of the Ni-containing compounds, **3** and **7**, show substantially more electron delocalization between the Ru atoms than the Pd and Pt analogues.

Acknowledgment. Support from the National University of Singapore as an Academic Research Fund Grant No. R-143-000-135/209-112 (L.Y.G.) and a postgraduate research scholarship (R.Y.C.S.) is gratefully acknowledged.

Supporting Information Available: Table S1, giving crystal data collection and processing parameters. Table S2, giving IR spectral data. Crystallographic data as CIF files for complexes **4A**, **5B**, **6**, and **8**−**10**. This material is available free of charge via the Internet at http://pubs.acs.org.

OM049407T

(18) (a) Kraatz, H.-B.; Boorman, P. M.; Hinman, A. S.; Ziegler, T.; Collison, D.; Mabbs, F. E. *J. Chem. Soc., Dalton Trans.* **1993**, 1665. (b) Thomas, K. R. J.; Chandrasekhar, V.; Zanello, P.; Laschi, F. *Polyhedron* **1997**, *16*, 1003. (c) Donzello, M. P.; Ercolani, C.; Kadish, K. M.; Ou, Z.; Russo, U. *Inorg. Chem.* **1998**, *37*, 3682. (d) Hori, A.; Mitsuka, Y.; Ohba, M.; Okawa, H. *Inorg. Chim. Acta* **2002**, *337*, 113. (e) Ali, M.; Ray, A.; Sheldrick, W. S.; Mayer-Figge, H.; Gao, S.; Sahmes, A. I. *New J. Chem*. **2004**, *28*, 412.